RSC Advances

ROYAL SOCIETY OF CHEMISTRY

www.rsc.org/advances

Journal Name

ARTICLE

Fast Lithium-ion Storage of Nb_2O_5 nanocrystals *in situ* Grown on Carbon Nanotubes for High-performance Asymmetric Supercapacitors

Received 00th January 20xx,
Accepted 00th January 20xx

DOI: 10.1039/x0xx00000x

www.rsc.org/

Xiaolei Wang,[a] Ge Li,[a] Ricky Tjandra,[a] Xingye Fan,[a] Xingcheng Xiao[b] and Aiping Yu*[a]

Lithium-ion supercapacitors have been attracting tremendous research interest due to significantly increased energy density. However, the power density and cycling stability are often sacrificed by poor conductivity and sluggish kinetics of transition metal oxides-based electrode. Herein, we report a composite material based on Nb_2O_5 nanocrystals *in-situ* grown on carbon nanotubes (CNTs) with a unique architecture exhibiting superior rate capability and long cycling stability. Even at 100 C-rate with charge/discharge time of 12 s, the composite still possesses a capacitance of ~160 C g^{-1}. A prototype of asymmetric lithium-ion supercapacitor composed of activated carbon cathode and CNT-Nb_2O_5 composite anode shows significantly improved energy density of ~50 Wh kg^{-1} with a power of 86.46 W kg^{-1}. Such composite materials with unique architecture hold great promise for future practical applications.

Introduction

The increasing concerns on rapid depletion of fossil oil and sustainability have brought tremendous research interest in energy storage systems such as lithium-ion batteries (LIBs) and supercapacitors.[1-4] Compared with LIBs, supercapacitors hold a number of properties including much higher power and long cycling life, which can complement or replace batteries.[5-8] However, typical electrochemical double-layer capacitors based on porous carbon materials with high surface area possess a capacitance of around 150 F g^{-1}, by storing charge at the interface of electrode and electrolyte.[9, 10] The resulting energy densities are generally a thousand times lower than those of LIBs. By comparison, pseudocapacitors based on inorganic non-carbon based materials store much higher charge (>1000 F g^{-1}) through reversible faradaic reactions.[11] Thus, seeking novel pseudocapacitive materials with high capacitance is one of the key research themes in this field.

So far, transition metal oxides have been extensively studied as a class of pseudocapacitive materials due to their different and high oxidation states, such as RuO_2,[12, 13] MnO_2,[14, 15] V_2O_5[16] and $Li_4Ti_5O_{12}$.[17, 18] Among various candidates, niobium pentoxide (Nb_2O_5) have been attracting tremendous research attention owing to its specific capacity of ~200 mA h g^{-1} and a comparatively low average operating potential (1.0~1.5 V *vs.* Li/Li^+).[19-21] Recently, it is reported that orthorhombic Nb_2O_5 exhibits an intercalation pseudocapacitance so that the charge storage is not limited by solid-state diffusion.[22, 23] However, similar to most transition metal oxides, Nb_2O_5 is known to suffer from intrinsically poor conductivity (~3×10^{-6} S cm^{-1} at room temperature),[24] which leads to electrodes with inferior power.

So far, many strategies are applied to overcome this barrier.[25-29] For example, utilizing a large amount of conductive agent (e.g. carbon black) can significantly increase electrode rate capability but sacrifice the overall capacitance. Although nanostructured materials such as mesoporous Nb_2O_5 thin film endow the electrodes with impressive rate performance,[25, 30] the low mass loading of the active material often leads to inferior energy density. It is well accepted that efficiently reducing ions diffusion and electrons migration paths and enhancing electronic conductivity are the key factors to achieving very high power rates.[31-33] Therefore, developing new materials with nanosized electroactive materials and conductive networks is highly demanded to improve the slow kinetics of Nb_2O_5-based electrodes, which is still a barrier to its practical application.

Recently, a new class of pseudocapacitive nanocomposite materials was developed for asymmetric supercapacitors by physically mixing Nb_2O_5 nanocrystals and carbon nanotubes (CNTs) followed by post-heat-treatment.[34] In this work, we report a facile solvo-thermal synthesis of CNT-Nb_2O_5 nanocomposites with superior rate capability, as well as long term cycling stability. As shown in **Scheme 1**, Nb_2O_5 nanocrystals (NCs) *in-situ* grow on CNTs scaffold, forming

[a] *Department of Chemical Engineering, University of Waterloo, 200 University Avenue West, Waterloo, Ontario N2M 5B2, Canada.*
[b] *Chemical Sciences and Materials Systems, General Motors Global Research and Development Center, 30500 Mound Road, Warren, Michigan 48090, United States.*
** Corresponding author: aipingyu@uwaterloo.ca, Tel: 1-(519)888-4567 EXT 38799*
† Electronic Supplementary Information (ESI) available: [details of any supplementary information available should be included here]. See DOI: 10.1039/x0xx00000x

intimate contact between the two components, while the further assembling results in a robust marimo-ball structure. This unique architecture offers several major features:[35, 36] (i) nanocrystals with low dimensions efficiently shortens lithium-ion diffusion length, leading to better utilization of Nb_2O_5; (ii) interconnected pores created by the CNTs network enables both effective electrolyte transport and fast active material accessibility; (iii) the *in-situ* growth ensures the intimate contacts and robust structure, endowing the electrode with high power density and cycling stability. High-performance prototype of asymmetric supercapacitor with the composite material-based anode and activated carbon-based cathode is fabricated, exhibiting both high energy and power density.

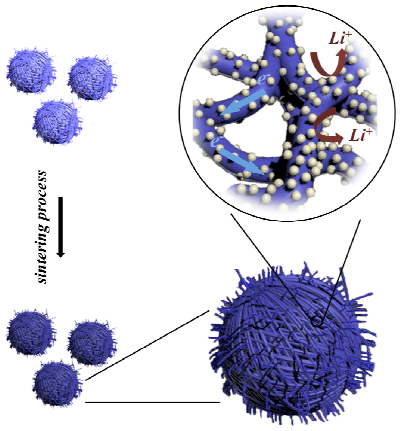

Scheme 1. Schematic of *in-situ* growing Nb_2O_5 nanocrystals on CNTs scaffold after post sintering proces.

Experimental

2.1 Synthesis of CNT-Nb_2O_5 nanocomposites:

Multi-wall carbon nanotubes were treated with acid by creating functional groups (e.g. carboxylic groups) through a similar method previously reported[37] A facile solvo-thermal synthesis was applied to produce CNT-Nb_2O_5 composites. Briefly, functionalized CNTs (75 mg) were homogeneously dispersed in ethanol (10 mL) by ultrasonicating for 30 min followed by stirring overnight. Niobium pentachloride (0.325 g) was dissolved in ethanol (4 mL) before mixed with above CNT dispersion under stirring for 30 min. The mixture was delivered to a 25 mL Teflon-lined autoclave and cooked for 12 hrs at 200 ºC. The resulted dark precipitates were collected by centrifuge, and further rinsed by ethanol and dried at 80 ºC for 12 hrs, and then sintered at 600 ºC for 4 hrs under N_2.

2.2 Material Characterization:

X-ray diffraction (XRD) measurements were conducted on an Inel XRG 3000 X-ray diffractometer (monochromatic Cu Kα X-rays). Nitrogen adsorption/desorption isotherms were collected on Micromeritics ASAP 2020 analyzer at 77 K. The Brunauer-Emmett-Teller (BET) method is applied to calculated the surface areas, while the Barrett-Joyner-Halenda (BJH) model is applied to determine the pore size distributions. Scanning electron microscopic (SEM) experiments were performed on a LEO FESEM-1530; while transmission electron microscopic (TEM), high-resolution TEM and EDX mapping images were obtained from a JEOL 2010F TEM/STEM field emission microscope in Canadian Center for Electron Microscopy (CCEM, McMaster University, Canada). X-ray photoelectron spectroscopy (XPS) data was collected from an AXIS Ultra DLD (Kratos Analytical Co. Ltd.).

2.3 Electrode Fabrication:

To prepare the slurry for electrode fabrication, the CNT-Nb_2O_5 nanocomposite powder, carbon black and polyvinylidenedifluoride (PVDF) binder were homogeneously dispersed in *N*-methylpyrrolidinone (NMP) in a mass ratio of 86:4:10. The homogenous slurry was drop-casted on copper foil current collector and dried at 100 ºC for 2 hrs. The electrodes were pressed at 2.0 MPa before further dried at 100 ºC overnight under vacuum. The mass loading of active materials was adjusted between 1.5 to 2.0 mg cm^{-2} on each electrode.

2.4 Electrochemical Measurements:

The electrodes were assembled into 2032-type coin cells in an argon-filled glovebox for electrochemical testings. In each coin cell, a piece of glass microfiber filter (Whatman, Grade GF/C) and a piece of lithium foil were used as separator and counter electrode, respectively, and 1 M $LiPF_6$ in a 1:1 (v/v) mixture of ethylene carbonate (EC) and dimethyl carbonate (DMC) was used as electrolyte. Cyclic voltammetric (CV) curves were collected on a VSP3 potentiostat/galvanostat (Bio-Logic LLC, Knoxville, TN) using cutoff voltages of 3.0 and 1.0 V (*vs.* Li/Li^+) at different scan rates. The galvanostatic charge/discharge measurements were performed on NEWARE BTS-CT3008 (Shenzhen Neware Technology, Co. Ltd., Shenzhen, China) at different current densities. The total charge or the specific capacitance of the composite electrodes is calculated based on the total mass of the composite materials. Electrochemical impedance spectroscopy measurement was conducted on a Princeton Applied Rsearch VersaSTAT MC potentiostat. The Nyquist plots were recorded potentiostatically by applying an AC voltage of 10 mV amplitude in the frequency range of 0.01 to 100k Hz. All electrochemical measurements were carried out at room temperature.

2.5 Prototype Asymmetric Supercapacitor Fabrication and Testing:

The asymmetric device was assembled using CNT-Nb_2O_5 nanocomposite based anode and activated carbon (AC) based cathode. The AC-based cathodes were fabricated by mixing AC, PVDF binder, and carbon black in the mass ratio of 8:1:1 in NMP before coated on aluminium foil. The ratio of CNT-Nb_2O_5 nanocomposite and activated carbon was controlled to be around 1:3.5 by mass. Asymmetric device was cycled at constant current between 3.0 and 0.5 V. The power density and energy density were calculated according to the total mass of anode and cathode materials, and a packaging factor of 0.4 was also applied. The energy density was determined by the equation $E = ½ CV^2$, where C

is the total capacitance and V is the maximum cell voltage, and power density was calculated using P = E/t., where P is the power density, t is the discharging time.

Results and Discussion

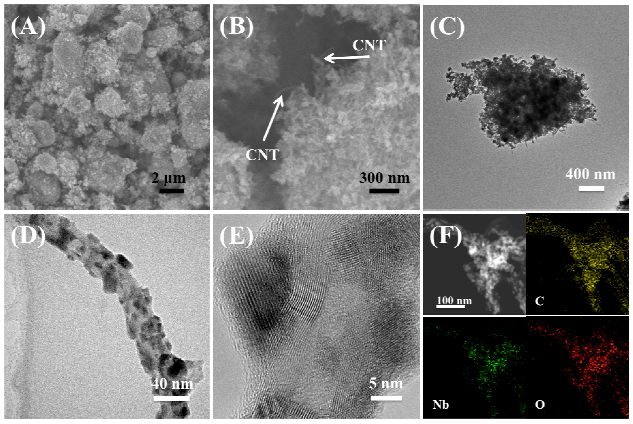

Figure 1. Representative (A) low- and (B) high-magnification SEM images of as-synthesized CNT-Nb_2O_5 nanocomposites with spherical shape; (C) TEM image of a single sphere of CNT-Nb_2O_5 nanocomposites; and (D) TEM image of part of a single CNT with *in-situ* grown Nb_2O_5 nanocrystals; (E) High-resolution TEM image of part of the composite; and (F) EDX mapping of elements C, O and Nb.

The structure of CNT-Nb_2O_5 nanocomposites can be revealed by scanning electron microscopic (SEM) and transmission electron microscopic (TEM). **Figure 1A** presents a representative SEM image of the as-synthesized CNT-Nb_2O_5 composites. Spherical morphology with marimo-like structure can be observed for most of the composite materials with sizes ranging from hundreds of nanometers to several microns. These micrometer-sized spheres facilitate the current electrode fabrication based on conventional slurry-coating process, which is compatible with industrial battery manufacturing. High-magnification SEM image in **Figure 1B** clearly reveals the detailed structure of the nanocomposites, where CNTs build a network spreading through the whole composites. **Figure 1C** presents a representative TEM image of a single composite sphere with the size of around 2 microns. The Nb_2O_5 NCs and CNTs are firmly combined, where no obvious separated and isolated NCs or CNTs can be observed, indicating a strong bonding between the two components. Moreover, the composite sphere also exhibits a hierarchically porous structure created from the entangled CNTs networks. The successful *in-situ* growth of Nb_2O_5 nanocrystals on CNTs was verified by high-magnification and high-resolution TEM in **Figure 1D** and **1E**. Nb_2O_5 nanocrystals with average size of ~10 nm grow on CNTs directly and uniformly (**Figure S-1** in the Electronic Supplementary Material (ESM)), with a lattice parameter of 0.39 nm, corresponding to the (001) plane of orthorhombic Nb_2O_5. **Figure 1F** shows EDX mapping images of the composite material. The well dispersed element Nb and O further confirms the uniform coating of Nb_2O_5 nanocrystals on the surface of CNTs and the intimate contact. Therefore, the low dimension of active Nb_2O_5 nanocrystals can efficiently shorten the ion-diffusion length, while the continuous and conductive scaffold and the intimate contacts between the two components can facilitate electron transportation. Therefore, such a unique architecture is highly desired for the electrodes with excellent lithium-storage ability.

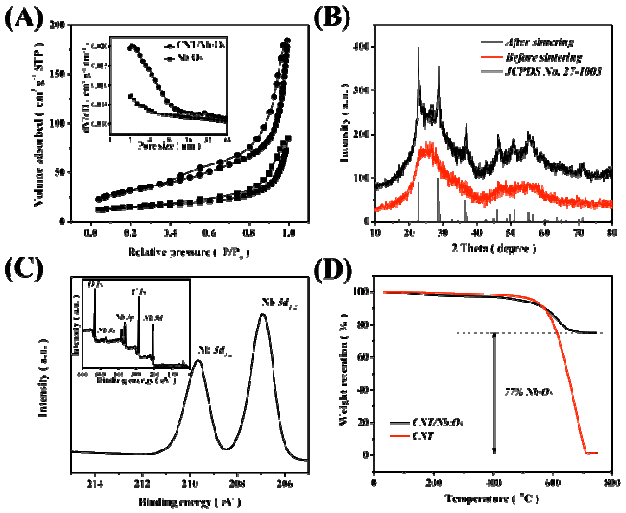

Figure 2. (A) Nitrogen adsorption-desorption isotherms of CNT-Nb_2O_5 nanocomposites and pure Nb_2O_5 (inset: pore-size distribution of CNT-Nb_2O_5 nanocomposites and pure Nb_2O_5); (B) XRD patterns of CNT-Nb_2O_5 nanocomposites before and after sintering process; (C) XPS core-level spectra of Nb $3d_{3/2}$ and Nb $3d_{1/2}$ peaks (inset: XPS survey spectrum of CNT-Nb_2O_5 nanocomposites); (D) TGA curves of CNTs and CNT-Nb_2O_5 nanocomposites.

The porous structure of the materials is characterized by analyzing the nitrogen adsorption-desorption isotherms (**Figure 2A**). A Brunauer–Emmett–Teller (BET) surface area was calculated to be 122 m^2 g^{-1} for CNT-Nb_2O_5 composites, while the pore size distribution is concentrated below 10 nm. In contrast, without the CNTs scaffold, pure Nb_2O_5 synthesized at the same condition gives a BET surface area of only 51 m^2 g^{-1}, which is close to that of the bulk material with average size of microns. Such a phenomenon suggests that the growth or aggregation of NCs can be effectively prevented by the existence of CNTs, which holds great importance in preserving the short ion-transport length. Furthermore, the porous feature and the high surface area endow the electrodes with efficient ion-transport and abundant active sites, respectively. **Figure 2B** compares the X-ray diffraction (XRD) patterns of CNT-Nb_2O_5 composite before and after sintering. After sintering process, the Nb_2O_5 NCs in CNT-Nb_2O_5 composites possess an orthorhombic crystal structure (JCPDS card No. 27-1003),[38, 39] which is the same as the pure Nb_2O_5 crystals synthesized in identical conditions without using CNTs (**Figure S-2** in the Electronic Supplementary Material (ESM)). The average domain size of Nb_2O_5 nanocrystals in the composites is around 9.82 nm calculated according to Scherrer's equation, which aligns well with the value from TEM observation. **Figure 2C** shows the X-ray photoelectron spectroscopic (XPS) results of CNT-Nb_2O_5 composite. Two well-defined peaks in the core level spectra at 209.7 and 206.9 eV respectively with an energy separation of 2.8 eV correspond to the Nb 3d of Nb_2O_5, which is consistent with previous reports, thus further confirms the

formation of Nb_2O_5.[40-42] **Figure 2D** presents the thermogravimetric analysis (TGA) results of pure CNTs and CNT-Nb_2O_5 composites. At temperature below around 500 ºC, the weight loss of CNTs can be negligible, while a steep weight loss can be observed between 550 to 700 ºC for both pure Nb_2O_5 and the composites due to the consumption of CNT. The composites consist of 77 wt.% of Nb_2O_5 and 24 wt.% of CNTs based on the TGA results. The mass ratio of Nb_2O_5 and CNTs can be easily adjusted to synthesize a class of composites with tunable properties. In this paper, we chose the composite material with 77 wt.% of Nb_2O_5 and 23 wt.% of CNTs to demonstrate the outstanding performance of *in-situ* growth of Nb_2O_5 on CNTs composites.

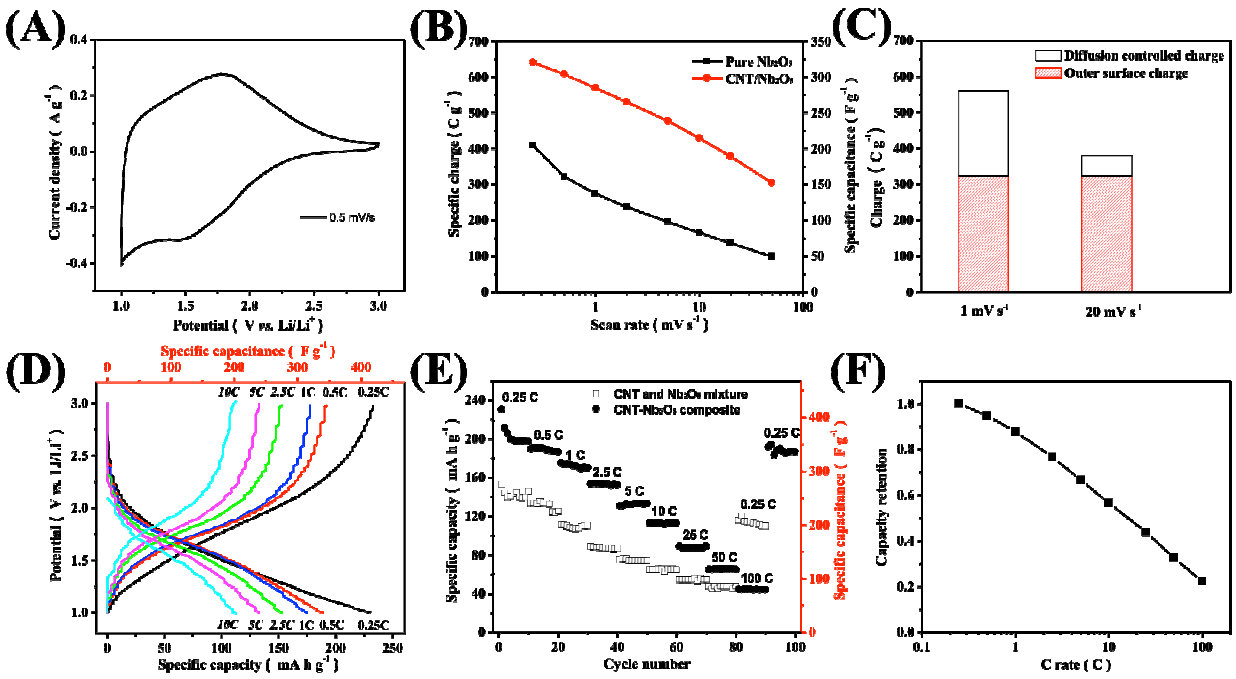

Figure 3. (A) Cyclic voltammograms of the CNT-Nb_2O_5 composites electrode at a scan rate of 0.5 mV s^{-1} with a cutting off voltage of 3.0 to 1.0 V *vs.* Li/Li^+ at room temperature; (B) Comparison of the rate capability of the CNT-Nb_2O_5 composite and pure Nb_2O_5 nanocrystals based electrodes; (C) Analysis of the total charge stored on the electrode based on CNT-Nb_2O_5 composite; (D) Galvanostatic charge/discharge profiles of CNT-Nb_2O_5 composite electrodes at various C-rates between 3.0 and 1.0 V; (E) Corresponding rate performance of the composite electrode; (F) Corresponding discharge capacity dependence on C-rates.

The electrochemical property of the CNT-Nb_2O_5 composites was analyzed by cyclic voltammetry (CV) using coin cells. Generally, the equation $Nb_2O_5 + xLi^+ + xe^- \leftrightarrow Li_xNb_2O_5$ is used to describe the Li^+ electrochemically intercalating and de-intercalating into and from Nb_2O_5, where x ($0<x<2$) represents the mole fraction of the intercalated Li^+. The typical cyclic voltammogram curves of the CNT-Nb_2O_5 composite at a scan rate of 0.5 mV s^{-1} is presented in **Figure 3A**. A couple of symmetric redox peaks can be found at ~1.5 V, which is consistent with Nb_2O_5-based materials,[21, 43], corresponding to the redox conversion between Nb^{5+} and Nb^{4+} by two Li^+. Moreover, the composite exhibits broader peaks, implying electrochemical reactions with broader distribution of energy[24], which is commonly observed in nanostructured materials. The total charge stored on the electrode can be calculated from the area within the CV curve. Charge storage of CNT-Nb_2O_5 composite was compared with pure Nb_2O_5 synthesized at identical condition at scan rate ranging from 1 to 50 mV s^{-1} (corresponding to charge/discharge times from 2000 to 40 s, respectively) (**Figure S-3** in the ESM). As shown in **Figure 3B**, obviously, the CNTs/Nb_2O_5 composite can store much more charge than the pure Nb_2O_5. At the same scan rate of 50 mV s^{-1}, the pure Nb_2O_5 only stores 31% (125 C g^{-1}, 62.5 F g^{-1}) of the total charge obtained at the scan rate of 1 mV s^{-1}, while the CNTs-Nb_2O_5 composite stores substantially more charge of 305 C g^{-1} (152.5 F g^{-1}), which is ~55% of the value at 1 mV s^{-1}.

In order to investigate how the *in-situ* growth of Nb_2O_5 onto conductive CNTs results in superior rate performance, Trasatti's method was applied to further analyze the contribution of the total stored charge.[44] As can be observed, the total stored charge q is strongly dependent on the scan rate (v), during which Li^+ slowly diffuses into the "inner" region from surface. According to the diffusion law, q has a linear relation to $v^{-1/2}$, which can be expressed by $q(v) = q_0 + constant*(v^{-1/2})$. Obviously, $constant*(v^{-1/2})$ is the diffusion-controlled charge, while q_0 is independent on scan rate, which represents the charge stored on the accessible outer surface, and can be calculated by plotting the $v^{-1/2}$ with total stored charge q.

Figure 3C displays the total stored charge on the electrodes at 1 and 20 mV s^{-1}, respectively. The composites possess not only more total charge but also significantly higher outer surface charge than the pure Nb_2O_5 (**Figure S-4** in the ESM). This result quantitatively indicates that building networks of CNTs with Nb_2O_5 nanocrystals allows more accessible surface sites of Nb_2O_5, which aligns well with the observed enhanced electron conductivity and rates performance.[34]

The excellent rate performance of CNT-Nb_2O_5 composite can also be observed from galvanostatic charge/discharge curves. **Figure 3D** shows charge and discharge profiles at various C-rates (1C = 200 mA $g_{composite}^{-1}$). In good alignment with other Nb_2O_5-based electrode, the typical sloped feature can be found, indicating the nature of intercalation-type redox reaction. In another word, the lithium intercalation remains a single-phase process after repeated cycling.[34] The initial discharge capacity at 0.25 C is 232 mA h g^{-1} (corresponding to ~418 F g^{-1} or ~835 C g^{-1}), corresponding to ~2.32 Li^+ intercalated into the composite. The CNT-Nb_2O_5 composite delivers a reversible capacity of 175 and 112 mA h g^{-1} (corresponding to 315 and 202 F g^{-1} or 630 and 403 C g^{-1}) at a rate of 1 C and 10 C, respectively. Interestingly, the composite still possesses a high capacity even at an extremely high rate. As shown in **Figure 3E** and **3F**, the composite still possesses a specific capacity of ~65 mA h g^{-1} (~117 F g^{-1} or ~234 C g^{-1}) at a rate of 50 C (corresponding to charge/discharge in 23 s). Even at 100 C (charge/discharge in 12 s), a capacity of ~44 mA h g^{-1} (~79 F g^{-1} or ~160 C g^{-1}) still remains.

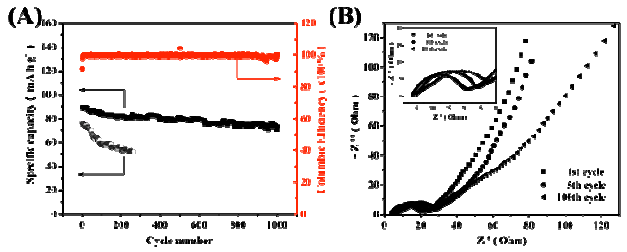

Figure 4. (A) Comparison of long-term cycling performance of the CNT-Nb_2O_5 composites and physically mixed Nb_2O_5 and CNTs at 10 C-rate; (B) Nyquist plots of the CNT-Nb_2O_5 nanocomposites electrode at 1st, 5th and 100th discharge/charge cycles over the frequency range from 100 kHz to 0.01 Hz. Inset shows enlarged spectra at high-frequency range.

The superior rate capability CNT-Nb_2O_5 is mainly attributed to the unique composite architecture, where Nb_2O_5 nanocrystals *in-situ* grow on the highly conductive CNTs networks. On one hand, the well-distributed Nb_2O_5 nanocrystals and porous CNTs networks create a large surface area, allowing fast accessibility of the active materials by electrolyte, while the low dimension of Nb_2O_5 materials efficiently shorten the Li^+ diffusion length. On the other hand, the *in-situ* growth ensures the intimate contact of Nb_2O_5 with highly conductive CNTs, which provides effective electron pathways. By comparison, physically mixed Nb_2O_5 nanocrystals and CNTs without any post-treatment leads to severe aggregation of the nanocrystals and poor contact between the active material with CNTs networks, showing an inferior rate capability (**Figure 3E**).

Besides the significant improvement of rate performance, the CNT-Nb_2O_5 also exhibits impressive cycling stability. The long-term cycling performance of the composite is shown in **Figure 4A**. A specific capacity of ~80 mA h g^{-1} remains (corresponding to ~288 C g^{-1}) after 1000 cycles at a current of 10 C-rate, corresponding to more than 80% of its initial value. The very slow capacity decay could be attributed to the gradual loss of active materials and irreversible reactions. By comparison, physically mixed Nb_2O_5 and CNTs without any treatment shows a poor cycling stability. At the same 10 C-rate, the mixture electrode shows a dramatic capacity deterioration after only 200 cycles. The excellent durability of the electrodes mainly lies on the robust architecture, which is confirmed by electrochemical impedance spectroscopy (EIS) analysis. **Figure 4B** shows the Nyquist plots of the composite electrode at different cycling status, where a single semicircle with a small intercept at high frequency range can be observed, implying a small ohmic and charge-transfer resistance. At low-frequency region, the Warburg tail possesses a moderately high slope, indicating the fast lithium-ion diffusion. After 100 cycles at high rate (10 C-rate), similar features can still remain, confirming the robust electrode structure, though a slight increase of charge-transfer and diffusion resistance can be observed from the low-frequency region. Nevertheless, the electrode preserves a small overall resistance due to the robust CNTs scaffold, which matches its excellent long-term cycling stability.

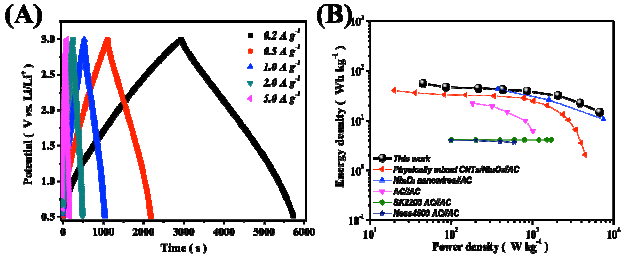

Figure 5. (A) Galvanostatic charge/discharge profiles of asymmetric supercapacitor with CNT-Nb_2O_5 composite anode and AC cathode at various current densities between 3.0 and 0.5 V; (B) Corresponding Ragone plot of the asymmetric supercapacitor and the comparison with activated carbon-based symmetric supercapacitor,[34, 45] physically mixed CNTs/Nb_2O_5 nanocrystals-AC asymmetric supercapacitor,[34] and Nb_2O_5 nanowires-AC asymmetric supercapacitor[46] reported in recent literatures. Generally, the mass of the electrode materials was estimated to be 40% of the total device weight, therefore a packaging factor of 0.4 was applied in this work.[6]

To further explore the feasibility to practically utilize CNT-Nb_2O_5 composite materials in the application of asymmetric supercapacitors, a full device was fabricated with composite material based anode and activated carbon based cathode. Based on the capacitance of each electrode as well as operation window, a mass ratio of cathode and anode of around 3.5:1 and a working window of 3.0-0.5 V were applied. **Figure 5A** shows the representative galvanostatic charge/discharge profiles of the asymmetric supercapacitor. A symmetric triangle shape can be obtained at various current densities with negligible IR drop, indicating a typical capacitive response of supercapacitors. To better demonstrate the device performance, Ragone plot in **Figure**

5B shows energy and power of CNT-Nb_2O_5 based asymmetric supercapacitor derived from constant current charge/discharge profiles. A high energy density of 47.17 Wh kg^{-1}can be reached, with a power density of 86.46 W kg^{-1}. Even at a high power of 6753.54 W kg^{-1} (corresponding to a discharging time of 7.6 s), the asymmetric supercapacitor still possesses the energy of 14.77 Wh kg^{-1}, indicating the high-power nature of supercapacitors can be well maintained. This type of asymmetric device exhibits significantly improved energy density compared with commonly used AC-based symmetric supercapacitors.[45] Moreover, such performance is even better than that of those asymmetric devices based on Nb_2O_5 materials involving either complex synthesis[46] or low electrode mass loading.[34].

Conclusions

We have successfully designed and developed high-performance electrode based on pseudocapacitive material of Nb_2O_5 nanocrystals *in-situ* grown on CNTs for supercapacitor applications. The composites show excellent rate capability and long cycling stability, which is mainly attributed to the unique composite architecture where low dimensional Nb_2O_5 nanocrystals have intimate contact with highly conductive and robust CNTs scaffold. The prototype of asymmetric supercapacitor has also been assembled using CNT-Nb_2O_5 composite-based anode and AC-based cathode, and shows impressing energy and power performance. It is expected that such a facile synthesis of the composite materials as well as the fabrication of asymmetric device hold great promise in developing practical next-generation high performance asymmetric supercapacitors.

Acknowledgements

This work was supported by the Natural Sciences and Engineering Research Council of Canada (NSERC), the University of Waterloo, and the Waterloo Institute for Nanotechnology. The authors also thank Canadian Center for Electron Microscopy (CCEM, McMaster University, Canada) for TEM characterization.

Notes and references

1. B. E. Conway, Kluwer Academic/Plenum Pblishers, New York, 1999, ch. 1, p. 29.
2. P. Simon and Y. Gogotsi, *Nat Mater*, 2008, **7**, 845-854.
3. Y.-M. Chiang, *Science*, 2010, **330**, 1485-1486.
4. K. Kang, Y. S. Meng, J. Breger, C. P. Grey and G. Ceder, *Science*, 2006, **311**, 977-980.
5. K. Naoi, W. Naoi, S. Aoyagi, J.-i. Miyamoto and T. Kamino, *Accounts of Chemical Research*, 2012, **46**, 1075-1083.
6. S. W. Lee, N. Yabuuchi, B. M. Gallant, S. Chen, B.-S. Kim, P. T. Hammond and Y. Shao-Horn, *Nat Nano*, 2010, **5**, 531-537.
7. A. S. Arico, P. Bruce, B. Scrosati, J.-M. Tarascon and W. van Schalkwijk, *Nat Mater*, 2005, **4**, 366-377.
8. V. Chabot, D. Higgins, A. Yu, X. Xiao, Z. Chen and J. Zhang, *Energy & Environmental Science*, 2014, **7**, 1564-1596.
9. L. L. Zhang and X. S. Zhao, *Chemical Society Reviews*, 2009, **38**, 2520-2531.
10. F. M. Hassan, V. Chabot, J. Li, B. K. Kim, L. Ricardez-Sandoval and A. Yu, *Journal of Materials Chemistry A*, 2013, **1**, 2904-2912.
11. V. Augustyn, P. Simon and B. Dunn, *Energy & Environmental Science*, 2014, **7**, 1597-1614.
12. J. P. Zheng and T. R. Jow, *Journal of Power Sources*, 1996, **62**, 155-159.
13. Z.-S. Wu, D.-W. Wang, W. Ren, J. Zhao, G. Zhou, F. Li and H.-M. Cheng, *Advanced Functional Materials*, 2010, **20**, 3595-3602.
14. G. Yu, L. Hu, N. Liu, H. Wang, M. Vosgueritchian, Y. Yang, Y. Cui and Z. Bao, *Nano Letters*, 2011, **11**, 4438-4442.
15. Z.-S. Wu, W. Ren, D.-W. Wang, F. Li, B. Liu and H.-M. Cheng, *ACS Nano*, 2010, **4**, 5835-5842.
16. Z. Chen, V. Augustyn, J. Wen, Y. Zhang, M. Shen, B. Dunn and Y. Lu, *Advanced Materials*, 2011, **23**, 791-795.
17. H.-G. Jung, S.-T. Myung, C. S. Yoon, S.-B. Son, K. H. Oh, K. Amine, B. Scrosati and Y.-K. Sun, *Energy & Environmental Science*, 2011, **4**, 1345-1351.
18. L. Shen, H. Li, E. Uchaker, X. Zhang and G. Cao, *Nano Letters*, 2012, **12**, 5673-5678.
19. J.-T. Han, D.-Q. Liu, S.-H. Song, Y. Kim and J. B. Goodenough, *Chemistry of Materials*, 2009, **21**, 4753-4755.
20. J.-T. Han, Y.-H. Huang and J. B. Goodenough, *Chemistry of Materials*, 2011, **23**, 2027-2029.
21. M. Wei, K. Wei, M. Ichihara and H. Zhou, *Electrochemistry Communications*, 2008, **10**, 980-983.
22. V. Augustyn, J. Come, M. A. Lowe, J. W. Kim, P.-L. Taberna, S. H. Tolbert, H. D. Abruna, P. Simon and B. Dunn, *Nat Mater*, 2013, **12**, 518-522.
23. J. W. Kim, V. Augustyn and B. Dunn, *Advanced Energy Materials*, 2012, **2**, 141-148.
24. A. L. Viet, M. V. Reddy, R. Jose, B. V. R. Chowdari and S. Ramakrishna, *The Journal of Physical Chemistry C*, 2009, **114**, 664-671.
25. E. Lim, H. Kim, C. Jo, J. Chun, K. Ku, S. Kim, H. I. Lee, I.-S. Nam, S. Yoon, K. Kang and J. Lee, *ACS Nano*, 2014, **8**, 8968-8978.
26. L. Kong, C. Zhang, S. Zhang, J. Wang, R. Cai, C. Lv, W. Qiao, L. Ling and D. Long, *Journal of Materials Chemistry A*, 2014, DOI: 10.1039/c4ta03604b.
27. G. Li, X. Wang and X. Ma, *Journal of Materials Chemistry A*, 2013, **1**, 12409-12412.
28. G. Li, X. Wang, Z. Chen, X. Ma and Y. Lu, *Electrochimica Acta*, 2013, **102**, 351-357.
29. G. Li, X. Wang and X. Ma, *Journal of Energy Chemistry*, 2013, **22**, 357-362.
30. K. Brezesinski, J. Wang, J. Haetge, C. Reitz, S. O. Steinmueller, S. H. Tolbert, B. M. Smarsly, B. Dunn and T. Brezesinski, *Journal of the American Chemical Society*, 2010, **132**, 6982-6990.
31. Z.-S. Wu, W. Ren, L. Xu, F. Li and H.-M. Cheng, *ACS Nano*, 2011, **5**, 5463-5471.
32. E. Frackowiak and F. Beguin, *Carbon*, 2001, **39**, 937-950.
33. C. Zhang, R. Maloney, M. R. Lukatskaya, M. Beidaghi, B. Dyatkin, E. Perre, D. Long, W. Qiao, B. Dunn and Y. Gogotsi, *Journal of Power Sources*, 2015, **274**, 121-129.
34. X. Wang, G. Li, Z. Chen, V. Augustyn, X. Ma, G. Wang, B. Dunn and Y. Lu, *Advanced Energy Materials*, 2011, **1**, 1089-1093.
35. Z. Chen, Y. Yuan, H. Zhou, X. Wang, Z. Gan, F. Wang and Y. Lu, *Advanced Materials*, 2014, **26**, 339-345.
36. Z. Chen, D. Zhang, X. Wang, X. Jia, F. Wei, H. Li and Y. Lu, *Advanced Materials*, 2012, **24**, 2030-2036.
37. C. Gao, C. D. Vo, Y. Z. Jin, W. Li and S. P. Armes, *Macromolecules*, 2005, **38**, 8634-8648.

38. J. He, Y. Hu, Z. Wang, W. Lu, S. Yang, G. Wu, Y. Wang, S. Wang, H. Gu and J. Wang, *Journal of Materials Chemistry C*, 2014, **2**, 8185-8190.
39. G. Park, N. Gunawardhana, C. Lee, S.-M. Lee, Y.-S. Lee and M. Yoshio, *Journal of Power Sources*, 2013, **236**, 145-150.
40. G. E. McGuire, G. K. Schweitzer and T. A. Carlson, *Inorganic Chemistry*, 1973, **12**, 2450-2453.
41. Z. Weibin, W. Weidong, W. Xueming, C. Xinlu, Y. Dawei, S. Changle, P. Liping, W. Yuying and B. Li, *Surface and Interface Analysis*, 2013, **45**, 1206-1210.
42. S. Qi, L. Fei, R. Zuo, Y. Wang and Y. Wu, *Journal of Materials Chemistry A*, 2014, **2**, 8190-8195.
43. L. Li, J. Deng, R. Yu, J. Chen, X. Wang and X. Xing, *Inorganic Chemistry*, 2010, **49**, 1397-1403.
44. S. Ardizzone, G. Fregonara and S. Trasatti, *Electrochimica Acta*, 1990, **35**, 263-267.
45. G. B. Appetecchi and P. P. Prosini, *Journal of Power Sources*, 2005, **146**, 793-797.
46. X. Wang, C. Yan, J. Yan, A. Sumboja and P. S. Lee, *Nano Energy*, 2015, **11**, 765-772.

Journal Name RSCPublishing

ARTICLE

Fast Lithium-ion Storage of Nb_2O_5 nanocrystals *in situ* Grown on Carbon Nanotubes for High-performance Asymmetric Supercapacitors

Xiaolei Wang,[a] Ge Li,[a] Ricky Tjandra,[a] Xingye Fan,[a] Xingcheng Xiao[b] and Aiping Yu[a]*

Nanocomposites of Nb_2O_5 nanocrystals *in situ* grown on CNTs are successfully developed and exhibit high specific capacitance and excellent rate capability due to the unique composite architecture, which led to successful fabrication of asymmetric supercapacitors with both high energy and power densities as well as long-term cycling stability.

Keyword: asymmetric supercapacitors; Nb_2O_5; carbon nanotubes; *in-situ* growth; high rate capability; high energy